Nano Energy (2014) 6, 10–18

Available online at www.sciencedirect.com

ScienceDirect

journal homepage: www.elsevier.com/locate/nanoenergy

RAPID COMMUNICATION

Significant performance enhancement of ZnO photoanodes from $Ni(OH)_2$ electrocatalyst nanosheets overcoating

Yanchao Mao[a,b], Hao Yang[a], Junxiang Chen[a], Jian Chen[c], Yexiang Tong[a,*], Xudong Wang[b,*]

[a]MOE Laboratory of Bioinorganic and Synthetic Chemistry, KLGHEI of Environment and Energy Chemistry, School of Chemistry and Chemical Engineering, Sun Yat-sen University, Guangzhou 510275, China
[b]Department of Materials Science and Engineering, University of Wisconsin-Madison, Madison, WI 53706, USA
[c]Instrumental Analysis and Research Centre, Sun Yat-Sen University, Guangzhou 510275, China

Received 14 February 2014; accepted 18 February 2014
Available online 12 March 2014

KEYWORDS
Photoelectrochemical water splitting;
Electrocatalyst;
ZnO;
$Ni(OH)_2$;
Core–shell nanorod arrays

Abstract: Designing high-performance photoanodes is essential for efficient solar energy conversion in photoelectrochemical (PEC) water splitting. In this paper, we report an effective approach to improve the PEC performance of ZnO nanorod (NR)-based photoanodes by introducing low-crystalline $Ni(OH)_2$ electrocatalyst nanosheets onto the ZnO surfaces. ZnO NR arrays and $Ni(OH)_2$ nanosheets were grown sequentially by electrochemical deposition, forming a core–shell structure. The ZnO NR cores acted as photon absorber as well as rapid charge transporter; whilst the wrinkled $Ni(OH)_2$ nanosheets largely increased the surface area and facilitated the PEC process by lowering the energy barrier of water oxidation and suppressing electron-hole recombination. As a result, more than one order of magnitude enhancement of PEC efficiency was obtained from the $Ni(OH)_2$/ZnO core–shell NR photoanode compared to bare ZnO NRs. The thickness effect of $Ni(OH)_2$ overcoating was also investigated. It was observed that although the electrocatalytic effect increased monotonically with the amount of $Ni(OH)_2$ coating, too much $Ni(OH)_2$ coverage could reduce the photocatalytic effect by limiting the light absorption. This research demonstrates that introducing appropriate amount of $Ni(OH)_2$ electrocatalysts can effectively facilitate the PEC performance of ZnO photoanodes. It suggests a promising route toward high-performance photoanode design for efficient solar energy conversion.

*Corresponding authors.
E-mail addresses: chedhx@mail.sysu.edu.cn (Y. Tong), xudong@engr.wisc.edu (X. Wang).

http://dx.doi.org/10.1016/j.nanoen.2014.02.008
2211-2855/

Introduction

Among numerous research efforts that have been devoted to efficient solar energy harvesting and conversion [1-3], photoelectrochemical (PEC) water splitting is a very attractive strategy for converting solar energy into hydrogen fuel [4-6]. Many semiconductor metal oxides, such as ZnO [7], TiO_2 [8], α-Fe_2O_3 [9], WO_3 [10], $BiVO_4$ [11], etc. have been studied as photoanodes in PEC applications, whereas tremendous challenge still exists in the development of effective and efficient photoanodes. An ideal photoanode requires high physical and chemical stability, appropriate band structure for broad-band light absorption and water redox reactions, high catalytic activity, as well as good charge transport property. In reality, there is no such material that can satisfy all these requirements for developing an ideal photoanode. For example, TiO_2 has excellent stability and catalytic property, and its valence and conduction bands straddle the water redox potentials. Therefore, TiO_2 has been widely used for photo water splitting, although its efficiency is still suffering from its low conductivity and wide bandgap that only allows UV-range photoactivity. α-Fe_2O_3 is recently proposed as a promising candidate due to its more appropriate band structure that enables water redox reactions in visible light regime. However, its insulator-like conductivity remains as a serious obstacle for achieving a high overall efficiency. ZnO has a very similar bandstructure as TiO_2 [4] with a typical electron mobility that is 10–100 times higher than that of TiO_2 [12-14]. Recent researches have also been conducted to dope or sensitize ZnO to enhance the light absorption and charge separation [14-19]. These merits make ZnO a very promising candidate for PEC water splitting, whereas, the reported solar-to-hydrogen conversion efficiency of ZnO photoanode is still considerably lower than TiO_2 due to its high recombination rate of photoexcited electron-hole pairs and poor surface activity for the oxygen evolution reaction [20-22].

Introducing electrocatalysts to the surface of photoanode has been suggested as an effective strategy to facilitate oxygen evolution reaction at the surface of photoanodes. For instance, Ni- and Co-based electrocatalysts have been widely used in electro-water splitting due to their high catalytic activity, chemical stability, and low toxicity [23-26]. Introducing Co-Pi film coating to the surface of oxide photoanode, such as α-Fe_2O_3 [27,28], WO_3 [29], and $BiVO_4$ [30], has recently been shown to be able to improve their PEC performance, due to the lower of water oxidation energy barrier at oxide surfaces by Co-Pi. A large variety of Ni based materials, such as nickel-dihydrolipoic acid [31], nickel hydroxides [32], and nickel oxides [33], also have received good attention as effective water splitting elector-catalysts. A robust solar water splitting system has been reported using CdSe nanocrystals capped with Ni^{2+}-dihydrolipoic acid catalysts [31]. It also has been found that a nickel oxide coated *n*-type silicon photoanode exhibited an enhanced PEC performance compared to the silicon photoanode under neutral pH condition [33]. Driven by these successful developments, we explored the application of Ni-based electrocatalysts in ZnO pohotoanode systems with an aim of overcoming the critical limitations that prevent ZnO from being an effective photoanode. Large-area $Ni(OH)_2$ nanosheet-coated ZnO core-shell nanorod (NR) arrays were synthesized *via* a well-controlled electrodeposition method. The $Ni(OH)_2$/ZnO NRs were used as the photoanode for PEC water splitting, exhibiting a drastic enhancement of photocurrent and conversion efficiency compared to bare ZnO NRs-based photoanodes. This work suggests introducing $Ni(OH)_2$ electrocatalysts can effectively improve the PEC performance of ZnO-based PEC photoanodes.

Experimental section

Synthesis of $Ni(OH)_2$/ZnO core-shell NR arrays

All reagents used in this study were analytical grade. Electrodeposition was carried out in a conventional three-electrode cell. A saturated calomel electrode (SCE) was used as the reference electrode, and the counter electrode was a graphite rod. The FTO glass with a sheet resistance of 14 Ω/sq was used as the working electrode. The FTO glass was cleaned in ultrasonic bath by deionized (DI) water, then ethanol, and finally rinsed DI water again before electrodeposition. The ZnO NR arrays were prepared *via* cathodic electrodeposition in a solution containing 0.02 M $Zn(NO_3)_2$+0.01 M CH_3COONH_4+ 0.01 M $(CH_2)_6N_4$ with a current density of 0.5 mA cm^{-2} at 90 °C for 1 h. The as-synthesized ZnO NR arrays were dried at room temperature in atmosphere. The electrodeposition of $Ni(OH)_2$ was then carried out on the as-synthesized ZnO NR arrays in a solution of 0.01 M $NiCl_2$ at 0.7 mA cm^{-2} at 90 °C with different electrodeposition times. After this two-step electrodeposition, the sample was rinsed in DI water, and then was dried in atmosphere at room temperature before the PEC measurement.

Characterizations

The morphology and structure of the samples was characterized using scanning electron microscope (SEM, LEO 1530) and transmission electron microscopy (TEM, JEM2010-HR). The TEM specimens were prepared by mechanically scratching off the NRs from substrate and collected by a carbon-coated copper grid. X-ray photoelectron spectroscopy (XPS) experiments were performed in an ESCA Lab 250 (Thermo VG) with 200 W Al Kα radiation. The analysis chamber pressure was $\sim 7.5 \times 10^{-6}$ Pa and the distance between the sample and X-ray gun was $\sim$1 cm. The pass energy constant was 20 eV for the high resolution scans. The binding energies were calibrated by placing the C 1 s peak of adventitious carbon at 284.8 eV.

PEC experiments

The PEC experiments were conducted on a CHI 660d electrochemical workstation (CHI Instruments) in a three-electrode PEC cell with a quartz window, through which simulated solar illumination was applied to the photoelectrode surface. A Pt foil and a Ag/AgCl electrode acted as the counter and reference electrodes, respectively. The as-prepared $Ni(OH)_2$/ZnO nanostructure on the FTO substrate was used as the working electrode. A 0.5 M Na_2SO_4 aqueous solution (pH=6.62) was used as the electrolyte. The illumination was provided by a 500 W Xe lamp (PLS-LAX500, Perfectlight) with a water IR filter. The illumination intensity at the sample position was determined to be 100 mW/cm^2. The PEC experiments were carried out in atmosphere at room temperature.

Results and discussion

The $Ni(OH)_2$/ZnO core-shell NR arrays were grown on FTO substrates *via* two-step electrodeposition, as schematically illustrated in Figure 1. First, ZnO NR arrays were grown on FTO substrates by cathodic electrodeposition. Their morphology is shown by a SEM image in Figure 2a. One hour deposition yielded dense hexagonal ZnO NRs uniformly covering the substrate surface. The NRs are ~1.5 μm long and ~300 nm in diameter with slightly tempered tips (Figure 2b). The NRs are quasi-aligned vertically due to their high density-confined orientation. Then, $Ni(OH)_2$ nanosheets were deposited onto the ZnO NRs through the same electrodeposition approach. The morphology of $Ni(OH)_2$ coating is shown in Figure 2c. All the ZnO NRs were uniformly covered with a rough layer of Ni $(OH)_2$. The $Ni(OH)_2$/ZnO NRs exhibit the same vertical alignment and no agglomeration was observed. A closer view shows that the $Ni(OH)_2$ coating had a sheet-like structure with a rough and wrinkled surface feature (Figure 2d). These wrinkles covered the entire NR body with a typically thickness of ~20 nm and a extention of ~100 nm. This unique coating structure tremendously increased the surface reaction sites compared to those provided by NRs, which is beneficial to high efficient PEC reactions.

XPS characterization was conducted to verify the chemical composition of the coating results. From the XPS spectrum, Zn, O, and Ni signals can be clearly identified (Figure 3a). Zn LMM and Ni KLL peaks are the Auger spectra related to the electrons of neighboring K, L and M atomic shells in Zn and Ni atoms, respectively. In addition, Cl signals were also detected, which came from adsorbed electrolyte during electrochemical deposit. The peak centered at 1022.1 eV corresponds to the Zn $2p_{3/2}$ core level and is the signature peak of Zn^{2+} in ZnO (Figure 3b) [34]. The symmetrical peak shape confirms the perfect stoichiometry of the electrodeposited ZnO NRs. The Ni 2p XPS spectrum is shown in Figure 3c. Two satellite peaks are located at the higher binding energy sides of the main double Ni 2p peaks. The peak shape and the Ni $2p_{3/2}$ peak value (856±0.1 eV) are in good agreement with literature reports confirming the state of Ni^{2+} in $Ni(OH)_2$ [35].

The $Ni(OH)_2$ coating morphology and its crystal structure was further investigated by TEM characterization. As shown in Figure 4a, $Ni(OH)_2$ nanosheets were rooted on the surface of ZnO NRs and extended ~100 nm above the surface. The large number of dark contrast stripes evidences the highly folded configuration of the nanosheets. Selected-area electron diffraction (SAED) pattern of the core-shell NR recorded one set of bright diffraction spots decorated with diffused halo diffraction rings (the inset of Figure 4a). The bright spots belong to the ZnO NR and confirm its single crystalline wurtzite structure. The diffused diffraction rings can be indexed to the hexagonal phase of $Ni(OH)_2$, suggesting the $Ni(OH)_2$ nanosheets were not fully developed polycrystalline structure. The $Ni(OH)_2$ nanosheets had very small thicknesses. By zooming in at the folded region, the smallest width of the dark contrast lines (corresponding to the nanosheet's thickness) was found to be ~3-4 nm (Figure 4b). The low crystallinity/amorphous structure of the nanosheet can also be clearly observed from the high-resolution TEM (HRTEM) image taken at the flat and folded regions (Figure 4c). Recently, superior electrocatalytic activity in oxygen evolution reaction from water was demonstrated from amorphous electrocatalytic materials compared to their crystalline phase due to their larger density of active unsaturated sites on the surface and higher degree of atomic structural flexibility than those of crystalline phases [36,37]. Meanwhile, the single crystal ZnO NR core can provide an effective electron transport pathway owing to its good conductivity [38,39]. Therefore, the configuration of low-crystalline $Ni(OH)_2$ nanosheet electrocatalyst shell on single-crystalline ZnO NR core is a promising photoanode structure that may significantly improve the performance of PEC water splitting.

PEC measurements were performed in 0.5 M Na_2SO_4 solution using a typical three-electrode electrochemical cell. The current density-voltage (*J-V*) curves shown in Figure 5a compare the PEC performances of ZnO NR and $Ni(OH)_2$/ZnO core-shell NR photoanodes. From the dark scans, bare ZnO NR photoanode exhibited a very low current density (~0.01 mA/cm^2 at 1.25 V) suggesting the good surface quality of the ZnO NRs. The dark current density of the $Ni(OH)_2$/ZnO photoanode at 1.25 V vs. Ag/AgCl was 1.68 mA/cm^2 (pH=6.62). The high current density in dark evidences the excellent electrocatalytic property of the $Ni(OH)_2$ nanosheets for oxygen evolution [23]. This dark current density value is also higher than that of Co-Pi/Co/Si electrode (~0.75 mA/cm^2 at 1.25 V vs. Ag/AgCl, pH=7) [40] and Co-Pi/α-Fe_2O_3 electrode (~0.9 mA/cm^2 at 1.25 V vs. Ag/AgCl, pH=8) [28]. Because more alkalescent electrolyte can promote the oxygen evolution reaction, the electrocatalytic property of the $Ni(OH)_2$/ZnO photoanode is indeed superior than these electrodes.

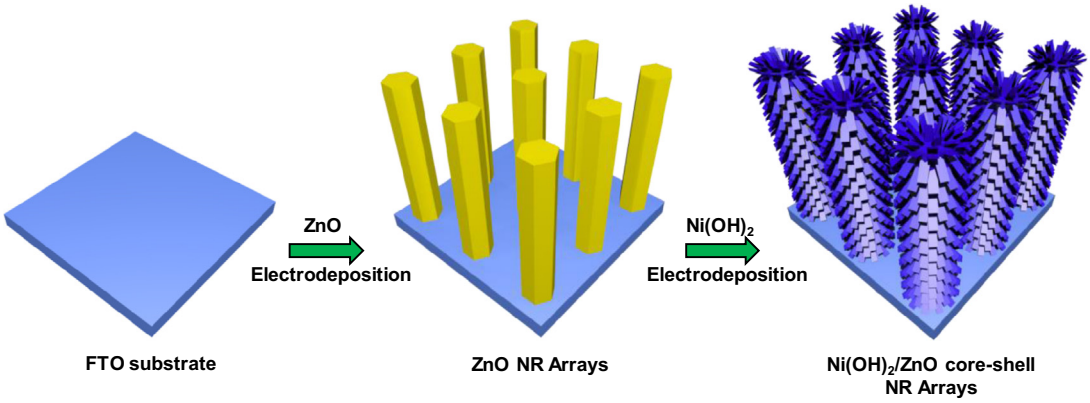

Figure 1 Schematic illustration of the fabrication procedures for $Ni(OH)_2$/ZnO core-shell NR arrays on FTO substrates.

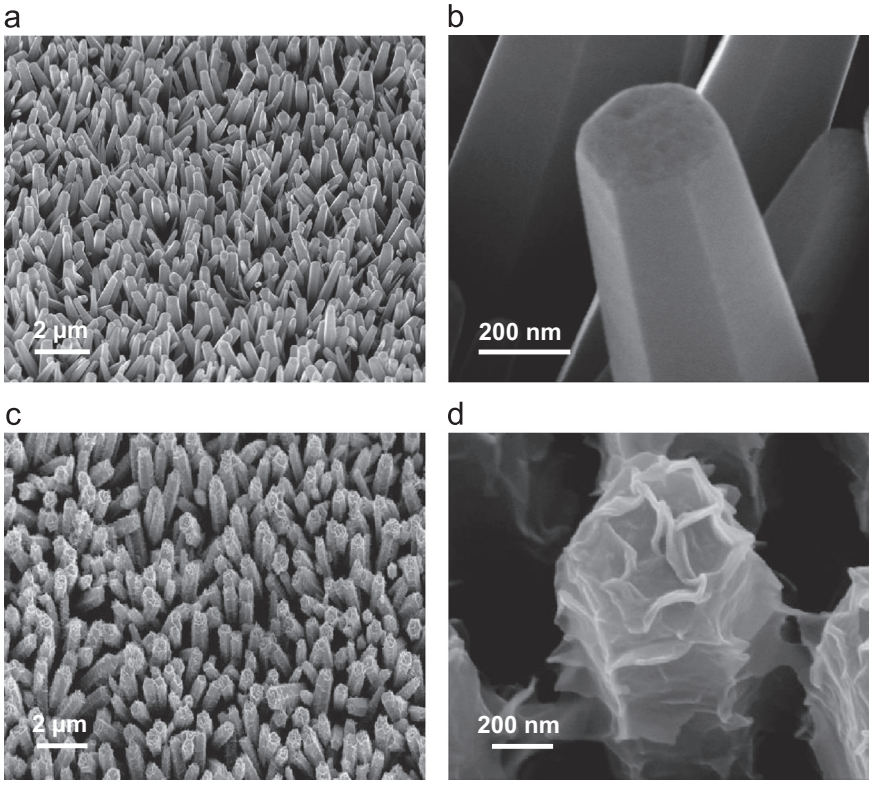

Figure 2 (a,b) Low- and high-magnification SEM images of as-synthesized ZnO NR arrays on FTO substrate, respectively. (c,d) Low- and high-magnification SEM images of $Ni(OH)_2$/ZnO core–shell NR arrays, respectively, with the $Ni(OH)_2$ electrodeposition time to be 5 min.

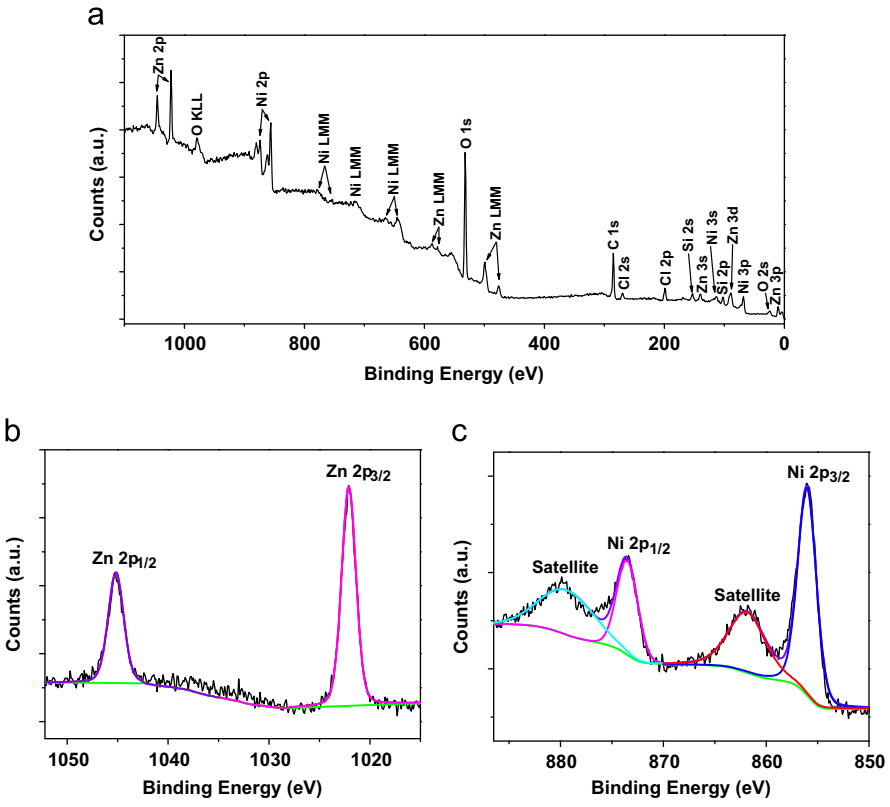

Figure 3 XPS spectrum of a survey scan (a), Zn 2p characteristics (b), and Ni 2p characteristics (c) of the $Ni(OH)_2$/ZnO core–shell NR arrays.

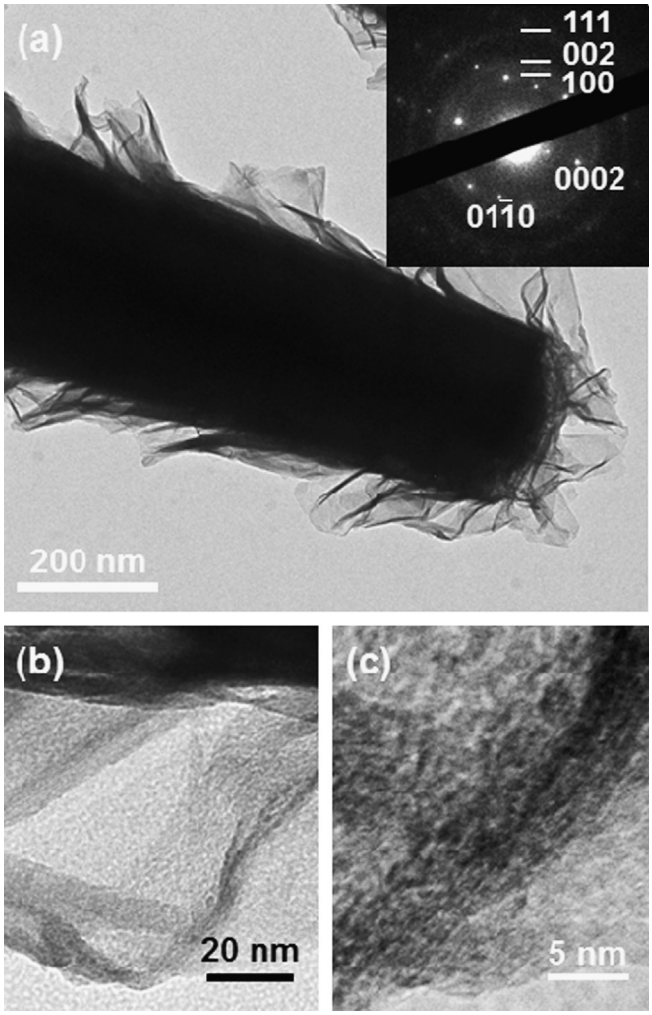

Figure 4 (a) TEM image of a $Ni(OH)_2$/ZnO core–shell NR. Inset is the corresponding SAED pattern. (b) TEM image showing the configuration of the outer $Ni(OH)_2$ nanosheet. (c) HRTEM image taken from the wrinkled region of the $Ni(OH)_2$ nanosheet.

Upon illumination by 100 mW/cm^2 white light, the total photocurrents (J_{total}) of both $Ni(OH)_2$/ZnO and bare ZnO photoanodes exhibited a significant increase. For ZnO photoanode, the J_{total} value at the potential of 1.25 V was 0.15 mA/cm^2 (inset of Figure 5a); whilst it was 2.58 mA/cm^2 for the $Ni(OH)_2$/ZnO photoanode at the same potential. All the samples were tested for at least 3 times, and no degradation in either performance or structure was observed. Upon $Ni(OH)_2$ coating, the J_{total} obviously shifted toward the negative potential direction compared. In our system, the thermodynamic potential for O_2 evolution E_{H_2O/O_2} is 0.64 V vs. the Ag/AgCl electrode at a pH of 6.62. Below this thermodynamic oxidation potential, enhancement of J_{total} also can be clearly observed. These characteristic improvements evidence the electrocatalytic effectof $Ni(OH)_2$ catalyst in PEC oxygen evolution reactions. Comparison between $Ni(OH)_2$-coated and bare ZnO NR photoanodes demonstrates that the $Ni(OH)_2$ electrocatalyst can effectively facilitate the PEC water splitting reactions on ZnO surfaces. The principle of such an electrocatalyst enhancement is schematically shown in Figure 5b. Upon illumination, electron–hole pairs are generated in ZnO by absorbing photons with energy higher than its band gap. For *n*-type ZnO photoanode, photogenerated electrons move from the conduction band (CB) to the conductive substrate and then reach the counter electrode to reduce water generating hydrogen. The photogenerated holes in the valance band (VB) of ZnO transfer to the $Ni(OH)_2$ shell that is in contact with ZnO surfaces. The holes are then trapped in $Ni(OH)_2$ and oxidize Ni^{II} into higher valence Ni^{III}/Ni^{IV}. The Ni^{III}/Ni^{IV} ions further interact with water molecules in their vicinity and generate oxygen; meanwhile, they are reduced back to Ni^{II} [23]. Introducing the $Ni^{II}/Ni^{III}/Ni^{IV}$ redox processes can largely reduce the energy barrier of water oxidation reactions by photogenerated holes, and thus significantly higher photocurrent can be obtained. In addition, adding a complete amorphous $Ni(OH)_2$ coating would effectively neutralize the surface trapping sites, and thus suppress the direct surface recombination of electron–hole pairs. Therefore, higher quantum efficiency of PEC water splitting can be expected.

The improvement induced by $Ni(OH)_2$ coating was quantified by identifying the net photocurrent density (J_{ph}), *i.e.* the difference between J_{total} and the dark current (Figure 5c), and corresponding PEC efficiency (Figure 5d). J_{ph} of the Ni$(OH)_2$/ZnO NR photoanode quickly rose when the applied bias was above 0.6 V and peaked at 1.18 V with a maximum value of 1.13 mA/cm^2. Then, J_{ph} decreased at higher applied bias. This is because the maximum photogenerated charge flux is fixed. Under large applied biases, electrocatalytic current exceeds the photogenerated charge flow and becomes the overwhelming effect. For bare ZnO NR photoanode, because it did not have electorcatalytic capability, its J_{ph} basically followed the same trend of its J_{total}. To compare, J_{ph} of the $Ni(OH)_2$/ZnO photoanode was nearly one order of magnitude larger than that of the bare ZnO photoanode. For instance, the maximum J_{ph} of $Ni(OH)_2$/ZnO and bare ZnO photoanodes were 1.13 mA/cm^2 and 0.14 mA/cm^2, respectively. Since the photocurrent onset potential was nearly unchanged after Ni$(OH)_2$ coating, similar to those observed from electorcatalyst/TiO_2 photoanode systems [41], water oxidation overpotential was used to compare the electrocatalytic reaction activities [42–44]. The overpotential values were calculated from the thermodynamic potential E_{H_2O/O_2}=0.64 V vs. Ag/AgCl at pH 6.62. The overpotential of the bare ZnO photoanode at a current density of 0.14 mA/cm^2 was found to be 0.64 V. The J_{ph} of the $Ni(OH)_2$/ZnO photoanode reached 0.14 mA/cm^2 at a more negative overpotential of 0.12 V, illustrating a higher activity of PEC oxygen evolution reaction. The solar-to-hydrogen conversion efficiencies (η) were calculated from the J_{ph} curves following equation [45]:

$$\eta(\%) = J_{ph}(1.23\text{-}E_{app})/P_{light}$$

where P_{light} is the power density of the illumination (100 mW/cm^2), and E_{app} is the absolute value of the applied bias that is added in series between the working and counter electrodes. Here, E_{app} is defined as ($E_m - E_{aoc}$), where E_m is the electrode potential (vs. Ag/AgCl) at which J_{ph} was measured, and E_{aoc} is the open circuit potential. The calculated PEC efficiency as a function of the applied bias is shown in Figure 5d, where the highest efficiency of the Ni$(OH)_2$/ZnO photoanode was found to be 0.43%, 10.8 times higher than that was produced by the bare ZnO photoanode

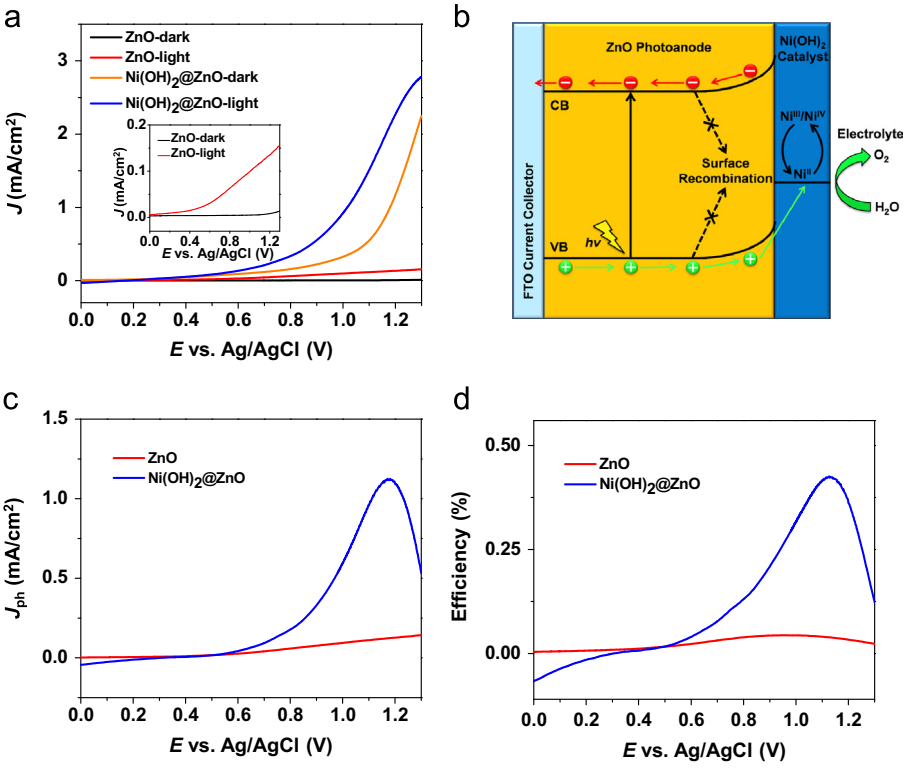

Figure 5 (a) Photocurrent and dark current curves of $Ni(OH)_2$/ZnO core-shell NR and bare ZnO NR photoanodes. Inset shows the magnified *J*-*V* curves of the bare ZnO photoanode. (b) Schematic diagram showing the kinetics of PEC water splitting by the $Ni(OH)_2$/ZnO core-shell NR photoanode. (c) The net photocurrent derived from the difference between the total photocurrent and the dark current of $Ni(OH)_2$/ZnO and ZnO photoanodes. (d) The calculated conversion efficiencies as a function of the applied bias for Ni $(OH)_2$/ZnO and ZnO photoanodes.

(0.04%). This efficiency is also a competitive value compared to other ZnO based photoanodes, such as undoped ZnO NRs (0.02%-0.08%) [17,46], N-doped ZnO NRs (0.1%) [46], N-doped ZnO nanowires (0.15%) [14], C-doped ZnO nanowires (0.18%) [16], $Zn_{0.96}Cu_{0.04}O$ NRs (0.21%) [47], ZnO nanosheets (0.27%) [48], and N-doped ZnO nanotetrapods (0.31%) [17]. This experiment clearly shows that introducing electrocatalysts to the surface of conventional oxide photoanodes can advantageously impact their PEC performance.

In order to further investigate the influence of $Ni(OH)_2$ electrocatalyst on the PEC performance of ZnO photoanodes, the amount and morphology of $Ni(OH)_2$ nanosheet were controlled by varying the deposition time between 1 and 7 min. Corresponding SEM images are shown in Figure 6. In the first minute, only a very thin $Ni(OH)_2$ film was conformally coated on the surface of ZnO NRs (Figure 6a). Small wrinkled area can be observed along corners and edges, from which the thickness of the $Ni(OH)_2$ nanosheet was estimated to be a few nm. Continuous growth of the Ni $(OH)_2$ nanosheets detached certain regions from the NR surface forming a rough and folded-sheet-like coating (Figure 6b). The folded area further grew larger and longer forming suspended $Ni(OH)_2$ nanosheets that were partially overlapping with each other (Figure 6c). This is the configuration used in our previous analysis. The length and thickness of $Ni(OH)_2$ nanosheets could grow continuously under extended deposition time, leading to a dense and thick coverage over the ZnO NRs (Figure 6d). The thickness of $Ni(OH)_2$ shells with different $Ni(OH)_2$ deposition times was obtained according to the SEM images in Figure 6. With the variable deposition times of $Ni(OH)_2$ for 1 min, 3 min, 5 min, and 7 min, the thickness of $Ni(OH)_2$ shell is about 20 nm, 40 nm, 100 nm, and 220 nm, respectively. All these different $Ni(OH)_2$ morphologies were applied as photoanodes to understand its influence on PEC performance.

Figure 7 shows *J*-*V*, J_{ph}, and PEC efficiencies of $Ni(OH)_2$/ZnO photoanodes with different $Ni(OH)_2$ deposition times and compared to bare ZnO photoanodes. Their performance parameters are also summarized in Table 1. As shown in Figure 7a, the dark current increased with the increasing of Ni $(OH)_2$ deposition time, indicating that increasing the amount of $Ni(OH)_2$ catalyst can directly enhance the electrocatalytic activity of oxygen evolution reactions. Accordingly, the J_{total} value also increased following the same trend. The $Ni(OH)_2$ enhancement to J_{ph} was compared in Figure 7b. The maximum J_{ph} increased from 0.5 mA/cm^2 to 1.13 mA/cm^2 as the deposition time of $Ni(OH)_2$ increased from 1 min to 5 min, and then decreased to 0.55 mA/cm^2 as the deposition time further increased to 7 min. The existence of optimal $Ni(OH)_2$ coating (or deposition time) is because that although more Ni $(OH)_2$ could generate higher electrocatalytic activity of oxygen evolution (evidenced by the monotonic increase of dark current), thicker $Ni(OH)_2$ nanosheet overcoating could also impair the light absorption in ZnO NRs and thus reduced the total number of photoexcited electron-hole pairs for water splitting. As shown in the inset of Figure 7b, J_{ph} of Ni $(OH)_2$/ZnO photoanodes were clearly enhanced below the thermodynamic potential E_{H_2O/O_2} =0.64 V (vs. Ag/AgCl, at pH

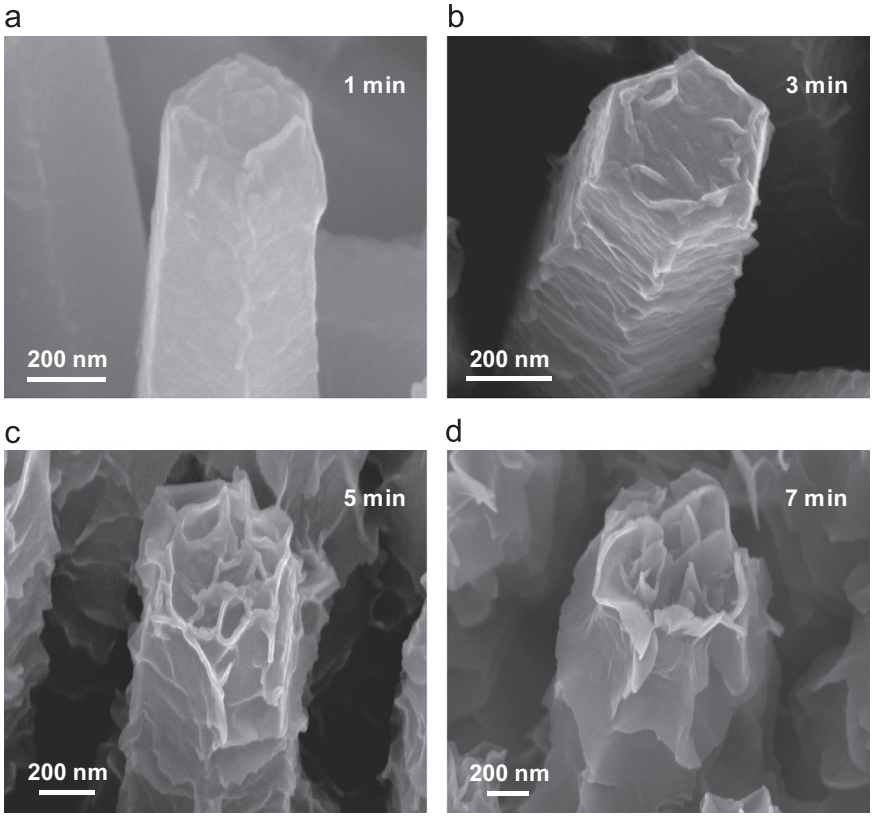

Figure 6 SEM images of $Ni(OH)_2$/ZnO core-shell NR arrays obtained with different $Ni(OH)_2$ deposition times: (a) 1 min, (b) 3 min, (c) 5 min, and (d) 7 min.

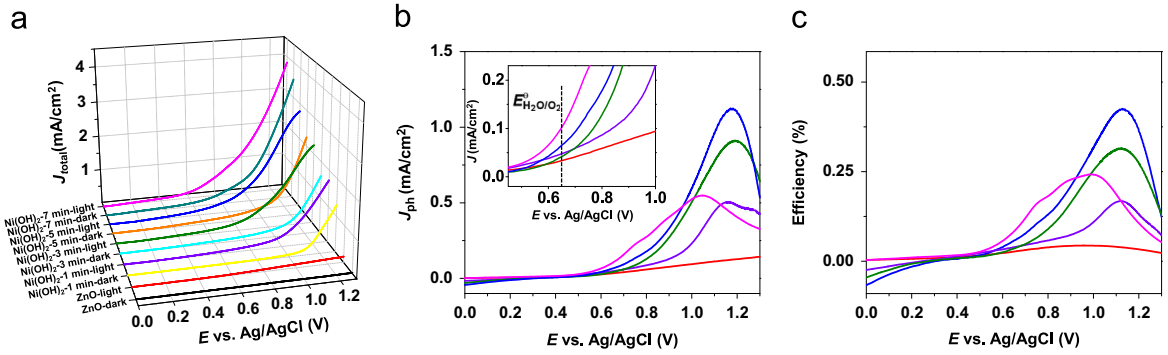

Figure 7 (a) *J*-*V*, (b) J_{ph}, and (c) PEC efficiencies of ZnO (red) and $Ni(OH)_2$/ZnO photoanodes with $Ni(OH)_2$ deposition time of 1 min (purple), 3 min (green), 5 min (blue), and 7 min (pink). Inset of (b) shows the magnified J_{ph} curves around the thermodynamic potiential E_{H_2O/O_2} =0.64 V vs. Ag/AgCl at pH 6.62.

Table 1 Summary of PEC performance of photoanodes made from ZnO NRs and $Ni(OH)_2$/ZnO core-shell NRs with different $Ni(OH)_2$ deposition times.

$Ni(OH)_2$ deposition time (min)	J_{dark} @ 1.25 V (mA/cm^2)	J_{total} @ 1.25 V (mA/cm^2)	$J_{ph,\ max}$ (mA/cm^2)	Overpotential @ J_{ph} of 0.14 mA/cm^2 (V)	η (%)
0 (bare ZnO)	0.01	0.15	0.14	0.64	0.04
1	0.95	1.41	0.50	0.28	0.17
3	1.21	2.04	0.91	0.17	0.31
5	1.68	2.58	1.13	0.12	0.43
7	2.93	3.29	0.55	0.05	0.24

6.62) compared to the bare ZnO photoanode. Meanwhile, the overpotential at $J_{ph}=0.14\ mA/cm^2$ decreased monotonically with the $Ni(OH)_2$ deposition time from 0.64 V for the bare ZnO photoanode to 0.05 V for the 7-min $Ni(OH)_2$ overcoated ZnO photoanode. It evidences the electrocatalytic property of the $Ni(OH)_2$ catalyst for water oxidation. Accordingly, the peak PEC efficiency increased from 0.17% to 0.43% as the deposition time of $Ni(OH)_2$ increased from 1 min to 5 min, and then dropped to 0.24% when the deposition time further increased to 7 min (Figure 7c). It is important to note that although J_{ph} and PEC efficiency various under different amount and morphology of $Ni(OH)_2$ nanosheet coating, all the values are significantly (at least >3 times) higher than that of bare ZnO photoanodes (Table 1). This observation strongly proved that introducing electrocatalysis can largely improve the PEC performance of conventional photoanodes.

Conclusion

In summary, we have developed a $Ni(OH)_2$/ZnO core–shell NR arrays photoanode for PEC water splitting *via* electrodeposition approach. The single-crystalline ZnO NR cores provide an effective electron transport pathway. The low-crystalline Ni $(OH)_2$ shell nanosheets covering the entire single-crystalline ZnO NR body served as electrocatalyst facilitating water oxidation reactions. This unique coating structure largely increased the surface reaction sites and significantly improved the PEC performance. The PEC efficiency of the $Ni(OH)_2$/ZnO photoanodes was obtained to be 0.43%, which was an order of magnitude increase compared to the bare ZnO photoanode (0.04%). The $Ni(OH)_2$/ZnO core–shell NR configuration has good potential as photoanodes for hydrogen generation *via* PEC water splitting. This research demonstrates that introducing electrocatalysts to conventional PEC photoanode systems and the complex low-crystalline/single-crystalline core–shell nanostructured configurations could open a new avenue toward designing and fabrication of high-performance PEC photoanodes.

Acknowledgments

X.W. thanks the financial support of NSF CMMI-1148919. Y.T. acknowledges the support of NSFC (91323101, 21273290 and J1103305), Natural Science Foundation of Guandong Province (S2013030013474), and the Research Fund for the Doctoral Program of Higher Education of China (No. 20120171110043). Y.M. thanks the China Scholarship Council for financial support.

References

[1] D.N. Congreve, J.Y. Lee, N.J. Thompson, E. Hontz, S.R. Yost, P.D. Reusswig, M.E. Bahlke, S. Reineke, T. Van Voorhis, M.A. Baldo, Science 340 (2013) 334.
[2] J. Shi, P. Zhao, X.D. Wang, Adv. Mater. 25 (2013) 916.
[3] Y.F. Wang, K.N. Li, Y.F. Xu, C.Y. Su, D.B. Kuang, Nano Energy 2 (2013) 1287–1293.
[4] M. Gratzel, Nature 414 (2001) 338.
[5] C. Cheng, H. Zhang, W. Ren, W. Dong, Y. Sun, Nano Energy 2 (2013) 779–786.
[6] J. Shi, Y. Hara, C. Sun, M.A. Anderson, X. Wang, Nano Lett. 11 (2011) 3413.
[7] J. Shi, M.B. Starr, H. Xiang, Y. Hara, M.A. Anderson, J.-H. Seo, Z. Ma, X. Wang, Nano Lett. 11 (2011) 5587.
[8] J. Shi, X.D. Wang, Energy Environ. Sci. 5 (2012) 7918.
[9] S. Shen, J. Jiang, P. Guo, C.X. Kronawitter, S.S. Mao, L. Guo, Nano Energy 1 (2012) 732.
[10] C. Santato, M. Odziemkowski, M. Ulmann, J. Augustynski, J. Am. Chem. Soc. 123 (2001) 10639.
[11] W.J. Luo, Z.S. Yang, Z.S. Li, J.Y. Zhang, J.G. Liu, Z.Y. Zhao, Z.Q. Wang, S.C. Yan, T. Yu, Z.G. Zou, Energy Environ. Sci. 4 (2011) 4046.
[12] E.M. Kaidashev, M. Lorenz, H. von Wenckstern, A. Rahm, H.C. Semmelhack, K.H. Han, G. Benndorf, C. Bundesmann, H. Hochmuth, M. Grundmann, Appl. Phys. Lett. 82 (2003) 3901.
[13] E. Hendry, M. Koeberg, B. O'Regan, M. Bonn, Nano Lett. 6 (2006) 755.
[14] X.Y. Yang, A. Wolcott, G.M. Wang, A. Sobo, R.C. Fitzmorris, F. Qian, J.Z. Zhang, Y. Li, Nano Lett. 9 (2009) 2331.
[15] Y.C. Qiu, K.Y. Yan, H. Deng, S.H. Yang, Nano Lett. 12 (2012) 407.
[16] S.T. Kochuveedu, Y.H. Jang, Y.J. Jang, D.H. Kim, J. Mater. Chem. A 1 (2013) 898.
[17] Y.F. Wei, L. Ke, J.H. Kong, H. Liu, Z.H. Jiao, X.H. Lu, H.J. Du, X.W. Sun, Nanotechnology 23 (2012) 235401.
[18] X.P. Qi, G.W. She, Y.Y. Liu, L.X. Mu, W.S. Shi, Chem. Commun. 48 (2012) 242.
[19] X.N. Wang, H.J. Zhu, Y.M. Xu, H. Wang, Y. Tao, S. Hark, X.D. Xiao, Q.A. Li, ACS Nano 4 (2010) 3302.
[20] Y.C. Lu, Y.H. Lin, D.J. Wang, L.L. Wang, T.F. Xie, T.F. Jiang, Nano Res. 4 (2011) 1144.
[21] L.L. Yang, Q.X. Zhao, M. Willander, X.J. Liu, M. Fahlman, J.H. Yang, Appl. Surf. Sci. 256 (2010) 3592.
[22] E.M.P. Steinmiller, K.S. Choi, Proc. Natl. Acad. Sci. 106 (2009) 20633.
[23] K. Juodkazis, J. Juodkazyte, R. Vilkauskaite, V. Jasulaitiene, J. Solid State Electrochem. 12 (2008) 1469.
[24] B.S. Yeo, A.T. Bell, J. Phys. Chem. C 116 (2012) 8394.
[25] M. Dinca, Y. Surendranath, D.G. Nocera, Proc. Natl. Acad. Sci. 107 (2010) 10337.
[26] Y. Surendranath, D.A. Lutterman, Y. Liu, D.G. Nocera, J. Am. Chem. Soc. 134 (2012) 6326.
[27] D.K. Zhong, J. Sun, H. Inumaru, D.R. Gamelin, J. Am. Chem. Soc. 131 (2009) 6086.
[28] D.K. Zhong, D.R. Gamelin, J. Am. Chem. Soc. 132 (2010) 4202.
[29] J.A. Seabold, K.S. Choi, Chem. Mater. 23 (2011) 1105.
[30] D.K. Zhong, S. Choi, D.R. Gamelin, J. Am. Chem. Soc. 133 (2011) 18370.
[31] Z. Han, F. Qiu, R. Eisenberg, P.L. Holland, T.D. Krauss, Science 338 (2012) 1321.
[32] G.M. Wang, Y.C. Ling, X.H. Lu, T. Zhai, F. Qian, Y.X. Tong, Y. Li, Nanoscale 5 (2013) 4129.
[33] K. Sun, N. Park, Z.L. Sun, J.G. Zhou, J. Wang, X.L. Pang, S. H. Shen, S.Y. Noh, Y. Jing, S.H. Jin, P.K.L. Yu, D.L. Wang, Energy Environ. Sci. 5 (2012) 7872.
[34] G. Deroubaix, P. Marcus, Surf. Interface Anal. 18 (1992) 39.
[35] N.S. McIntyre, M.G. Cook, Anal. Chem. 47 (1975) 2208.
[36] R.D.L. Smith, M.S. Prevot, R.D. Fagan, Z.P. Zhang, P.A. Sedach, M.K.J. Siu, S. Trudel, C.P. Berlinguette, Science 340 (2013) 60.
[37] E. Tsuji, A. Imanishi, K. Fukui, Y. Nakato, Electrochim. Acta 56 (2011) 2009.
[38] Y.B. He, G.R. Li, Z.L. Wang, C.Y. Su, Y.X. Tong, Energy Environ. Sci. 4 (2011) 1288.
[39] P.H. Yang, X. Xiao, Y.Z. Li, Y. Ding, P.F. Qiang, X.H. Tan, W.J. Mai, Z.Y. Lin, W.Z. Wu, T.Q. Li, H.Y. Jin, P.Y. Liu, J. Zhou, C.P. Wong, Z.L. Wang, ACS Nano 7 (2013) 2617.

[40] E.R. Young, R. Costi, S. Paydavosi, D.G. Nocera, V. Bulovic, Energy Environ. Sci. 4 (2011) 2058.
[41] M. Bledowski, L. Wang, A. Ramakrishnan, A. Bétard, O. V. Khavryuchenko, R. Beranek, ChemPhysChem 13 (2012) 3018.
[42] H. Tüysüz, Y. Hwang, S. Khan, A. Asiri, P. Yang, Nano Res. 6 (2013) 47.
[43] T. Nakagawa, C.A. Beasley, R.W. Murray, J. Phys. Chem. C 113 (2009) 12958.
[44] A.J. Esswein, M.J. McMurdo, P.N. Ross, A.T. Bell, T.D. Tilley, J. Phys. Chem. C 113 (2009) 15068.
[45] S.U.M. Khan, M. Al-Shahry, W.B. Ingler, Science 297 (2002) 2243.
[46] O. Game, U. Singh, A.A. Gupta, A. Suryawanshi, A. Banpurkar, S. Ogale, J. Mater. Chem. 22 (2012) 17302.
[47] Y.K. Hsu, C.M. Lin, Electrochim. Acta 74 (2012) 73.
[48] Y.K. Hsu, Y.G. Lin, Y.C. Chen, Electrochem. Commun. 13 (2011) 1383.

Yanchao Mao is a PhD candidate in the School of Chemistry and Chemical Engineering of Sun Yat-sen University and also currently a visiting student in the Department of Materials Science and Engineering at University of Wisconsin-Madison. His research focuses on fabrication of nanomaterials for photoelectrochemical water splitting and nanogenerator based self-powered systems.

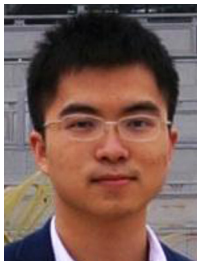

Hao Yang majored in Material Chemistry at the School of Chemistry and Chemical Engineering and received his BS degree in 2009 at Sun Yat-Sen University. He joined Prof. Yexiang Tong's group in 2012 and became a graduate in the same group. His current research interests focus on the design of nanomaterials for fuel cell and solar energy conversion.

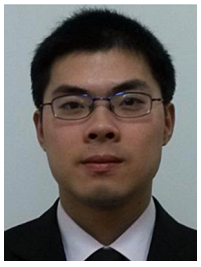

Junxiang Chen received his BS degree in Material Chemistry from the School of Chemistry and Chemical Engineering at Sun Yat-sen University in 2009. He joined Professor Yexiang Tong's group in 2012 and his research mainly focuses on the design of nanomaterials for solar energy conversion.

Dr. Jian Chen received his PhD degree in Physics from Sun Yat-sen University in 2001. He is currently a professor in Instrumentation Analysis and Research Center, Sun Yat-sen University, Guangzhou, China. His research interests are focused on the structure characteristic and compositions of the material surface and interface. He has co-authored more than 100 journal papers. He received China National Nature & Science Award 2001 and other awards for his research.

Dr. Yexiang Tong received his BS in General Chemistry in 1985, MS in Physical Chemistry in 1988, and PhD in Organic Chemistry in 1999 from Sun Yat-sen University. He joined Sun Yat-sen University as an assistant professor of Chemistry in 1988. He was granted the Talents Cultivated by "Thousand-Hundred-Ten" Program of Guangdong Province in 1996, the Secretary-General of Guangdong Chemical Society in 2009, and the councilman Chinese Chemical Society in 2010. His current research focuses on the electrochemical synthesis of alloys, intermetallic compounds and metal oxide nanomaterials, and investigation of their applications for energy conversion and storage.

Dr. Xudong Wang is an assistant professor in the department of Materials Science and Engineering at University of Wisconsin-Madison. His research interests include studying the growth and assembly of oxide nanowire arrays, understanding the coupling effect of semiconductor properties and piezoelectric charge displacement, and developing nanogenerator that uses piezoelectric nanomaterials to convert low level mechanical energy into electricity. He has published 70 papers in peer reviewed scientific journals, contributed 7 book chapters in his research field, and holds 5 patents/provisional patents on oxide nanostructures and nanomaterial-enhanced energy harvesting. His publications have been cited over 6,000 times by peers and his current h-index is 34.